

Electrodisintegration of ^{58}Ni , ^{60}Ni , and ^{62}Ni

E. Wolyneć,* W. R. Dodge, R. G. Leicht,[†] and E. Hayward

National Bureau of Standards, Washington, D.C. 20234

(Received 30 January 1980)

The (e,p) and (e,α) cross sections for targets of ^{58}Ni , ^{60}Ni , and ^{62}Ni have been measured in the electron energy range 16–100 MeV. They have been analyzed using the distorted-wave Born approximation $E1$ and $E2$ virtual photon spectra. Protons are emitted primarily following $E1$ absorption but α -emission results from a combination of $E1$ and $E2$ absorption.

[NUCLEAR REACTIONS $^{58,60,62}\text{Ni}(e,p)$ and $^{58,60,62}\text{Ni}(e,\alpha)$; measured $\sigma(E_0, E_x, 48^\circ)$, $\sigma(E_0, E_x, 90^\circ)$, $\sigma(E_0, E_x, 132^\circ)$; obtained $\sigma(e,p)$, $\sigma(e,\alpha)$; deduced $\sigma_{\gamma,p}^{E1}(E)$, $\sigma_{\gamma,\alpha}^{E1}(E)$, $\sigma_{\gamma,\alpha}^{E2}(E)$.]

I. INTRODUCTION

The work described here has already been reported^{1,2}; the main conclusions have been altered to reflect changes in our cross sections owing to a more careful analysis of our experimental data and to more sophisticated techniques in extracting $E1$ and $E2$ multipole strengths. Here we describe an experiment in which the (e,p) and (e,α) cross section for targets of ^{58}Ni , ^{60}Ni , and ^{62}Ni have been measured in the electron energy range 16–100 MeV. These have been analyzed, by making use of the virtual photon spectra, to obtain the photonuclear cross sections for electric dipole and quadrupole absorption that result in proton and α -particle emission. Photodisintegration using bremsstrahlung was also studied as an additional constraint on the multipolarity assignments.

In electron scattering experiments nuclear excitations are studied by measuring the spectra of scattered electrons at some angle to the incident electron beam. These data are then analyzed in terms of the momentum transfer to the nucleus; no information is obtained concerning the charged particles, neutrons, or γ rays emitted in the deexcitation of the nucleus. The complementary experiment is to study these deexcitation products, in which case the experiment integrates over the momentum transfers of the outgoing electron. In the work reported here the charged particles, protons, and α particles were studied. Since most of the data taken in this experiment involved electron energies only up to 50 MeV, the nuclear interactions were dominated by the transverse, photonlike components.

In electroexcitation the nucleus absorbs the radiation emitted by the electron in a single interaction. The multipole decomposition of this radiation has been studied by Gargaro and Onley³ and further developed by Soto Vargas, Onley, and

Wright.⁴ In their formulation the cross section for some nuclear excitation $\sigma_{e,x}(E_0)$, produced by an electron of total energy E_0 , may be written as

$$\sigma_{e,x}(E_0) = \int_0^{E_0-m} \sum_{\lambda L} \sigma_{\gamma,x}^{\lambda L}(E) N^{\lambda L}(E_0, E, Z) \frac{dE}{E}, \quad (1)$$

where $\sigma_{\gamma,x}^{\lambda L}(E)$ is the photonuclear absorption cross section for the same nuclear excitation for photons of energy E and multipolarity λL , and $N^{\lambda L}(E_0, E, Z)$ represents the virtual photon intensity spectrum generated when an electron of energy E_0 interacts with a target nucleus of atomic number Z . In the work to be described here $\sigma_{\gamma,x}^{\lambda L}(E)$ will stand for the $E1$ or $E2$ partial giant resonance cross sections resulting in the emission of protons or α particles. The magnitudes and shapes of the virtual

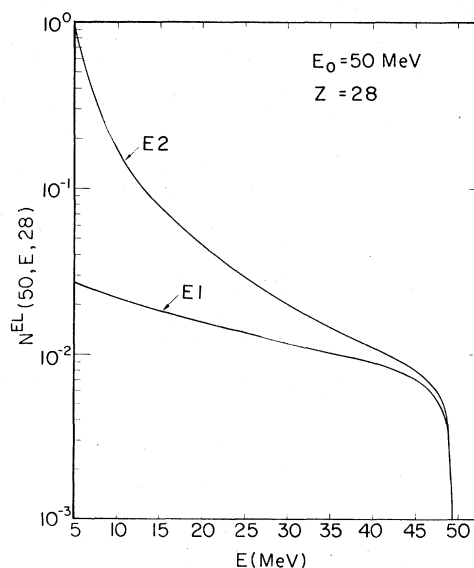


FIG. 1. The intensity spectra of $E1$ and $E2$ virtual photons generated when 50 MeV electrons are inelastically scattered by a Ni nucleus.

photon spectra have been calculated by Gargaro and Onley³ using the distorted-wave Born approximation (DWBA) which takes into account the distortion of the incoming and outgoing electron waves in a point nuclear Coulomb field. It is immediately apparent (see Fig. 1) that the $E2$ virtual photon spectrum is much richer than the $E1$ spectrum in photons in the giant resonance region. Bremsstrahlung, on the other hand, contains all multipoles in equal amounts. These differences are crucial to the analysis employed here.

Equation (1) is the defining equation for the virtual photon spectrum $N^{\lambda L}(E_0, E, Z)$. For forward electron scattering the momentum transfer q approaches E and the reduced matrix elements for photo and electrodisintegration are exactly the same.^{5, 6} This simplification has permitted Onley and his collaborators to calculate the virtual photon spectra without recourse to a nuclear model. This entire development then rests on the long wavelength approximation which we take to be $qR \ll 1$, R being the radius of the radiating system. This is a good approximation for electric dipole excitations in which the electrons are scattered into very small angles. The same is also true for electric quadrupole transitions up to electron energies of perhaps 50 MeV. The excitation of higher multipoles requires larger momentum transfers and for them the concept of the virtual photon spectrum generated by point nucleus must be viewed with great caution. The electric monopole mode⁷ can also be excited by electrons. It obviously cannot be related to a photodisintegration cross section according to Eq. (1) but must be described in terms of its own matrix element.⁸

At the present time the electric dipole virtual photon spectrum can be used with some confidence because (1) it has been verified in experiments in which the ratios of cross sections produced by electrons and positrons were obtained⁹ and (2) the cross section for the reaction $^{238}\text{U}(e, n)^{237}\text{U}$ has been shown¹⁰ to bear the proper relationship to the $^{238}\text{U}(\gamma, n)^{237}\text{U}$ cross section.

The idea that the giant dipole resonance decays mainly by nucleon emission and that α decay is more important for the giant isoscalar $E2$ resonance has already been expressed.^{11, 12} It will be shown that this concept is borne out, at least in part, for the nickel isotopes.

The electrodisintegration of a series of light elements resulting in proton emission has already been studied by Dodge and Barber.¹³ In a similar experiment Barber and Vanhuyse¹⁴ explored four heavy targets. The (e, α) reactions have been studied by Murphy *et al.*,^{15, 16} Dodge and Vander Molen,¹⁷ Tamae *et al.*,¹⁸ and a group at Glasgow.¹⁹

There have been several experimental studies

of the nickel isotopes that related even more directly to the present work. Ishkanov *et al.*, have measured the photoproton spectra and determined the (γ, p) cross sections for ^{58}Ni and ^{60}Ni .^{20, 21} Carver and Turchinets have obtained the (γ, p) cross sections in ^{58}Ni and ^{62}Ni by an activation technique.²² In an experiment very similar to the one described here, Miyase *et al.*,²³ have determined the (γ, p) and (γ, p_0) cross sections in ^{58}Ni , ^{60}Ni , and ^{62}Ni by studying the (e, p) reaction. Finally, the proton capture reaction $^{59}\text{Co}(p, \gamma_0)$ of Diener *et al.*²⁴ also yields the (γ, p_0) cross section. ^{60}Ni was one of the targets in the survey of (e, α) cross sections of Tamae *et al.*,¹⁸ and Flowers *et al.*²⁵ have also studied this reaction. Otherwise the relevant existing data come from the capture reactions $^{54}\text{Fe}(\alpha, \gamma_0)^{58}\text{Ni}$ (Ref. 12) and $^{56}\text{Fe}(\alpha, \gamma_0)^{60}\text{Ni}$.²⁶

II. EXPERIMENTAL DETAILS

The differential cross sections $d^2\sigma/d\Omega dT$ for the electroproduction of protons and α particles from targets of ^{58}Ni , ^{60}Ni , and ^{62}Ni have been measured at 48° , 90° , and 132° using incident electron energies in the range 16–50 MeV. The protons and α particles were momentum analyzed and identified by means of a magnetic spectrometer having circular counters, approximately 2.3 cm in diameter, in its focal plane.²⁷ The beam was monitored using ferrite toroids that were, in turn, calibrated with respect to a Faraday cup.

The separated isotope foils, nominally 2 mg/cm² in thickness, were purchased from the Oak Ridge National Laboratory. Table I gives their thicknesses and purities. These quantities were verified by elastic electron scattering. A thinner ^{60}Ni foil was also studied.

Additional, very useful information can be obtained if a radiator is interposed in the electron beam ahead of the target so that the outgoing particles are now generated by electrodisintegration plus the bremsstrahlung from the radiator. The power of this method is that it allows us to change the multipole composition of the radiation seen by the target. For nickel and the energies involved here, the virtual photon spectrum contains about four times as many $E2$ as $E1$ photons, but the

TABLE I. Target properties.

Isotope	Purity %	Thickness mg/cm ²
58	99.8	1.97
60	99.8	1.88
62	98.7	2.07
60		1.05

bremsstrahlung beam, being a plane wave, contains all multipoles in equal intensity.

For electron energies in the range 35–50 MeV a second experiment was performed. A radiator, 217 mg/cm² of Ta, was interposed in the beam 7.6 cm ahead of the Ni target but out of view of the spectrometer. The electrons multiple scatter in the radiator enlarging the beam-spot size and altering the effective momentum acceptance interval of our circular focal plane detectors. A correction was made for these effects based on a Monte Carlo calculation verified by an experimental study of the yields as a function of radiator thickness and distance from the target. This exercise resulted in a correction to the radiator data which increased these yields by about 10% at 35 MeV and 5% at 50 MeV.

Systematic data were not taken above 50 MeV because the point nucleus approximation may no longer be adequate for the *E2* virtual photon spectra. Cross sections were measured at the single energy of 100 MeV; they will be used in the following to demonstrate roughly the magnitude of the nuclear size effects.

III. RESULTS

A. The spectra

Figures 2(a) and 3(a) show the doubly differential cross sections $d^2\sigma/d\Omega dT$ for the emission of α particles at 90° and protons at 90° and 132° when 50 MeV electrons are incident on targets of ⁵⁸Ni, ⁶⁰Ni, and ⁶²Ni. These are shown as typical examples, similar data having been obtained at other electron energies and at several angles. It can be seen at once that the α -particle yields from ⁵⁸Ni and ⁶⁰Ni are essentially the same; that from ⁶²Ni being about half as much. The corresponding proton yields, on the other hand, are in the ratio 1/0.4/0.2. The extraordinarily large proton yield from ⁵⁸Ni is, of course, associated with its well-established^{28–30} low photoneutron cross section. We can anticipate that, when measured, the photoneutron cross section for ⁶²Ni will be correspondingly large.

All of the spectra are similar in shape having a broad peak near 5 MeV for the protons and 8 MeV for the α particles with the asymmetry characteristic of Coulomb barrier penetration. Above 25 MeV there are no dramatic changes as the electron energy increases; the high energy tail becomes slightly more important but always represents a small fraction of the total cross section. This suggests that most of the yield results from photon absorption at giant resonance energies and that the decay modes are essentially statistical in nature. Similar proton spectra have been obtained by

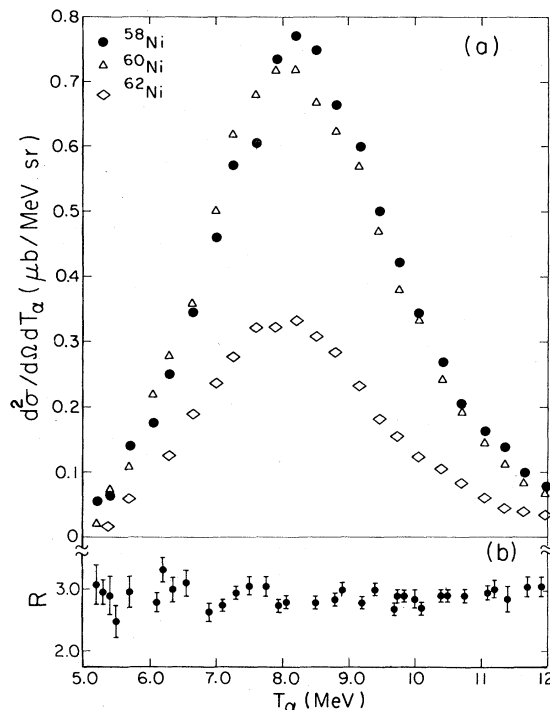


FIG. 2. (a) The α spectra $d^2\sigma/dT_\alpha d\Omega$ measured at 90° when 50 MeV electrons are incident on targets of ⁵⁸Ni, ⁶⁰Ni, and ⁶²Ni. (b) The ratio of the number of α particles produced by electro plus photodisintegration in ⁵⁸Ni to the number produced by electrodisintegration alone. This ratio was obtained by placing a 0.217 g/cm² Ta radiator in the beam ahead of the ⁵⁸Ni target.

Ishkhanov *et al.*²¹ who have studied ⁵⁸Ni and ⁶⁰Ni and shown that essentially the same proton spectra come from different excitation energies. Three groups^{15,16,18,19} have measured alpha spectra from a number of targets in experiments similar to the present one; the low energy components of these spectra have been interpreted in terms of a statistical model.

The protons in the peak are isotropic though the high energy tail is peaked forward of 90°. This effect is already noticeable in ^{60,62}Ni for 8 MeV protons as may be seen in the insert of Fig. 3(a). The α -particle angular distributions will be discussed later on.

Figures 2(b) and 3(b) show for ⁵⁸Ni the ratios of the number of α particles or protons observed with the radiator in to the number obtained with the radiator out. The constancy of this ratio, as a function of the kinetic energy of the emerging particle, shows that the spectra generated in electro and photodisintegration are very nearly the same. The radiator increases the intensity by an amount that depends on the resonance energies and the multipole composition of the ab-

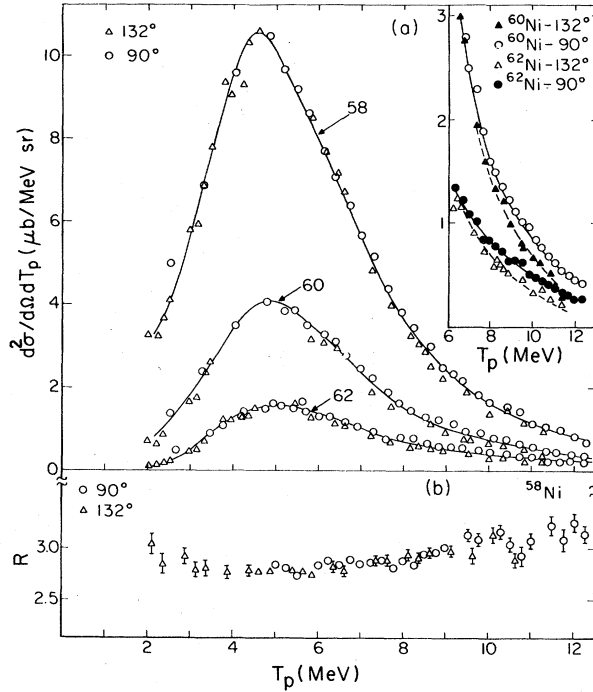


FIG. 3. (a) The proton spectra $d^2\sigma/dT_p d\Omega$ measured at 90° and 132° when 50 MeV electrons are incident on targets of ^{58}Ni , ^{60}Ni , and ^{62}Ni . The insert shows the tails of the energy spectra for ^{60}Ni and ^{62}Ni where the protons are slightly forward peaked. (b) The ratio of the number of protons produced by electro plus photodisintegration in ^{58}Ni to the number produced by electrodisintegration alone. This ratio was determined by placing a 0.217 g/cm^2 Ta radiator in the beam 7.6 cm ahead of the ^{58}Ni target.

sorbed radiation. Similar results were obtained for $^{60,62}\text{Ni}$.

Flowers *et al.*²⁵ have found a narrow peak near 4.2 MeV in their ^{60}Ni α spectra which they interpret as arising from the onset of neutron emission. This feature was not apparent in our data obtained using the 2 mg/cm^2 Oak Ridge target so a thinner target was made at NBS. A low energy α peak was then observed. Analysis of this foil by electron scattering revealed that it contained F, C, and O; it had been sprayed with a substance containing Teflon to facilitate the rolling operation. Murphy *et al.*¹⁶ have pointed out that the contamination of metal targets with low- Z nuclei such as oxygen is a common problem; Flowers³¹ confirms that the Glasgow target is thus afflicted.

B. The (γ, p) cross sections

Protons and α particles of the same energy can be counted simultaneously in the spectrometer. Since the (e, α) cross section is much smaller than the (e, p) cross section and has its peak for

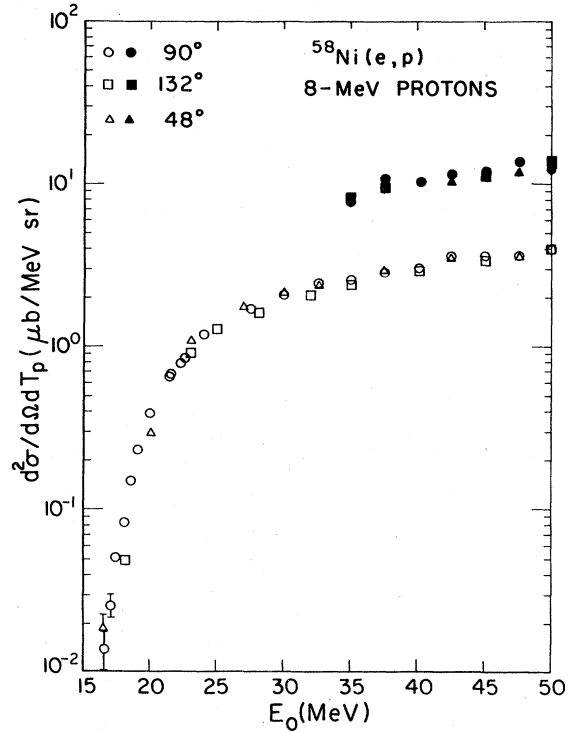


FIG. 4. The differential cross section $d^2\sigma/dT_p d\Omega$ for the production of 8 MeV protons from ^{58}Ni as a function of total incident electron energy E_0 . The data were taken at three angles: 132° (squares), 90° (circles), and 48° (triangles). The upper points refer to the yields resulting from electro plus photodisintegration when a 0.217 g/cm^2 Ta foil is interposed in the electron beam.

$E_\alpha = 8 \text{ MeV}$, it seemed practical to measure the proton and α -particle yield curves by counting an energy band near 8 MeV as a function of the total incident electron energy E_0 in the range 16–50 MeV. The yield curve $\sigma(E_0, \theta)$ vs E_0 for 8 MeV protons emitted by ^{58}Ni as a function of incident electron energy is shown in Fig. 4. The measurements were made at 48° , 90° , and 132° and the angular distribution may be seen to be isotropic for all but the lowest energy electrons used. The upper points for E_0 between 35 and 50 MeV, were obtained by interposing the 0.217 g/cm^2 tantalum radiator in the electron beam ahead of the ^{58}Ni target so that the protons are produced by the both electro and photodisintegration. These data have been corrected as described above.

The cross section $\sigma_{e,p}(E_0)$ was then obtained (see Fig. 5) by comparing the area under the proton differential cross section shown in Fig. 3 with the number in the energy band near 8 MeV and by multiplying the differential cross section by 4π . The yields $Y_{e,p}(E_0)$ with the radiator in were obtained in the same units by multiplying by the same constant. The justification for this procedure lies

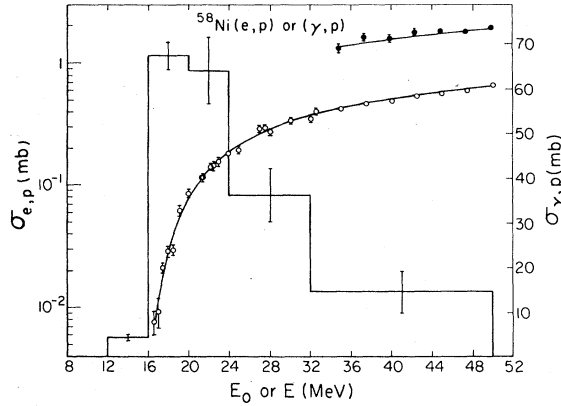


FIG. 5. The cross section (left-hand scale) for the production of protons $\sigma_{e,p}(E_0)$ when electrons of total energy E_0 are incident on a ^{58}Ni target (open circles). The closed circles represent the yield of protons obtained when a 0.217 g/cm^2 Ta foil was interposed in the incident electron beam. The latter have been corrected for the changes in geometry produced by the multiple scattering of the electrons in the radiator. The lines drawn through the points result from folding the histogram, representing the (γ,p) cross section (right-hand scale), with the $E1$ virtual photon spectrum in Eq. (1) and using the Davies-Bethe-Maximon cross section in Eq. (2).

in the fact that at 90° the ratio of the number of 8 MeV protons to the total number in the spectrum is the same with the radiator in or out.

The relationship between our measured electrodisintegration cross section and the corresponding photodisintegration cross section is given by Eq. (1). The corresponding expression for the yield with the radiator in is

$$Y_{e,x}(E_0) = \sigma_{e,x}(E_0 - 2\Delta E_0) + N_r \int_0^{E_0 - m} \sum_{\lambda L} \sigma_{\gamma,x}^{\lambda L}(E) K(E_0 - \Delta E_0, E) \frac{dE}{E}, \quad (2)$$

where N_r is the number of nuclei/cm 2 in the tantalum radiator, $K(E_0, E)$ is the bremsstrahlung cross section in tantalum, and ΔE_0 is the energy an electron loses in traversing half the radiator thickness.

The cross sections $\sigma_{e,p}(E_0)$ and yields $Y_{e,p}(E_0)$ were fit using various photonuclear cross section shapes along with the $E1$ DWBA virtual photon spectra in Eqs. (1) and (2). Both the Schiff³² and Davies-Bethe-Maximon³³ bremsstrahlung cross sections were used in Eq. (2), and since these cross sections differ in magnitude³⁴ by nearly 10%, this choice determines the size of the derived integrated (γ,p) cross sections.

Since the $E1$ virtual photon spectrum is relatively flat (see Fig. 1), the fits to the (e,p) cross section are not very sensitive to the assumed

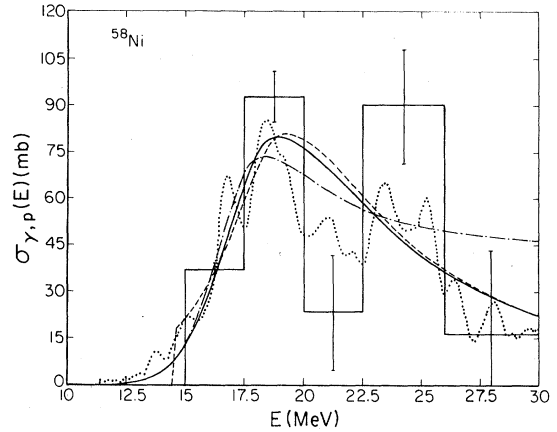


FIG. 6. Various (γ,p) cross section shapes that fit the $^{58}\text{Ni}(e,p)$ data when combined with the $E1$ virtual photon spectrum in Eq. (8). Here only the electrodisintegration data below 30 MeV have been used. The dotted curve represents the data of Ref. 17 multiplied by 1.22. The dashed curve is a Lorentz line having a smaller width below the resonance energy than above and truncated near 15 MeV. The solid curve has a Gaussian shape below and a Lorentz shape above the resonance energy. The dot-dashed curve is a Gaussian below the resonance energy and a Lorentz line plus a constant above. The histogram with 2.5 MeV bins roughly reproduces the structure in the measured (γ,p) cross section.

shape of the $\sigma_{\gamma,p}^{E1}(E_0)$; the fits are sensitive to the giant resonance energy and even more to the magnitude of the integrated cross section. Figure 6 demonstrates this insensitivity. The five photonuclear cross section shapes shown there produce equally good fits to the electrodisintegration data. The dotted curve represents 1.22 times the measured (γ,p) cross section of Ref. 20, and the three smooth curves are various analytic representations of the cross section. The histogram with 2.5 MeV bins roughly reproduces the structure in the measured (γ,p) cross section. As a result of this study and other tests, we arrived at the "histogram" fit as the fairest way to present the results as it does not impose any particular line shape on the cross section. This fitting procedure, which is really equivalent to a coarse unfolding, gave the best fit with the smallest number of free parameters.

The curves $\sigma_{e,p}(E_0)$ and $Y_{e,p}(E_0)$ were simultaneously fit by representing the (γ,p) cross section as a histogram. The excitation energy was divided into bins 4 MeV wide below 24 MeV and much wider above that energy. The data then choose the cross section magnitudes appropriate to these bins. The fits and the corresponding derived (γ,p) cross sections are shown in Figs. 5, 7, and 8 for ^{58}Ni , ^{60}Ni , and ^{62}Ni , respectively. These fits are based on the use of the Davies-

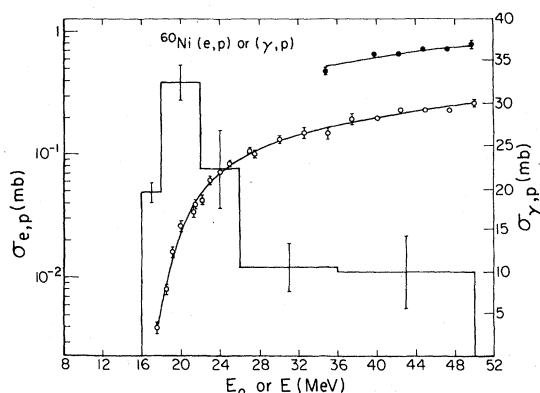


FIG. 7. The cross section (left-hand scale) for the production of protons $\sigma_{e,p}(E_0)$ when electrons of total energy E_0 are incident on a ^{60}Ni target (open circles). The closed circles represent the yield of protons obtained when a 0.217 g/cm^2 Ta foil was interposed in the incident electron beam. The latter have been corrected for the changes in geometry produced by the multiple scattering of the electrons in the radiator. The lines drawn through the points result from folding the histogram, representing the (γ, p) cross section (right-hand scale), with the $E1$ virtual photon spectrum in Eq. (1) and using the Davies-Bethe-Maximon cross section in Eq. (2).

Bethe-Maximon bremsstrahlung cross section with the Fermi-Thomas model screening functions.³⁴ The use of the Schiff bremsstrahlung cross section [formula 3BS(e) of Ref. 35] leads to slightly smaller magnitudes for the integrated (γ, p) cross section. The integrated cross sections obtained using the two bremsstrahlung cross sections are compared in Table II. Based on guidance provided by Tseng and Pratt,³⁶ we believe that the truth lies somewhere in between but closer to the Davies-Bethe-Maximon result.

Table III compares the cross sections integrated to 30 MeV with other values available in the litera-

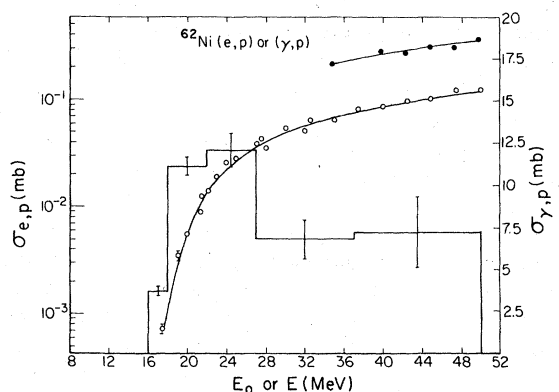


FIG. 8. The $\sigma_{e,p}(E_0)$ and $Y_{e,p}(E_0)$ for ^{62}Ni (left-hand scale) obtained by using the $E1$ virtual photon spectrum in Eq. (1) and the Davies-Bethe-Maximon bremsstrahlung cross section in Eq. (2).

TABLE II. Percentage of a dipole sum in the proton channel. $\int_0^{30} dE = 60NZ/A \text{ MeV mb}$; upper limit of the integral = 50 MeV.

Nucleus	Schiff	D-B-M
^{58}Ni	113 ± 11	126 ± 12
^{60}Ni	53 ± 6	61 ± 7
^{62}Ni	28 ± 2	32 ± 2

ture. Carver and Turchinets²² measured the γ, p cross sections of ^{58}Ni and ^{62}Ni using an activation technique. Their integrated cross section magnitudes should be smaller than those obtained in the other experiments in which protons were counted, since the latter also include the integrated (γ, pn) cross sections and, perhaps even more important, the $(\gamma, p\alpha)$ and $(\gamma, 2p)$ cross sections. The results of Miyase *et al.*²³ are somewhat lower than the other measurements; this discrepancy cannot result from the fact that they have used the virtual photon spectrum calculated in the plane wave approximation to analyze their data. It is also worth pointing out that the ground-state cross sections reported in Ref. 23 are less than 5% of the total (γ, p) cross sections.

As a check on our absolute cross section magnitudes, we have also measured the (e, p) cross section for ^{62}Ni at 30 MeV using an activation technique. We chose ^{62}Ni because of the convenient 100-min half life of ^{61}Co as well as its simple decay scheme; the beta decay populates the first excited state of ^{61}Ni at 67 keV 100% of the time, 14% of the γ rays being internally converted.³⁷ This was a completely independent measurement. The ^{62}Ni target was exposed for 3 h to

TABLE III. Integrated (γ, p) cross sections.

Nucleus	$\int_0^{30} \sigma_{\gamma,p}(E) dE$ (MeV mb)	Reference
^{58}Ni	570 ± 60	20
	520 ± 90	22
	480 ± 100	23
	754 ± 75^a	This work
	800 ± 92^b	This work
^{60}Ni	320 ± 50	20
	210 ± 80	23
	264 ± 29^a	This work
	307 ± 43^b	This work
^{62}Ni	110 ± 25	23
	130 ± 20	22
	120 ± 9^a	This work
	133 ± 14^b	This work

^a Using the Schiff cross section.

^b Using the Davies-Bethe-Maximon cross section.

about 8 μA of 30 MeV electrons. As in a previous, similar experiment³⁸ the electron charge was measured in 100-s intervals using a nonintercepting toroid which was then compared with a Faraday cup whose absolute calibration is known. The 67 keV gamma ray was counted using the calibrated planar Ge(Li) detector system³⁹ developed by the NBS Radioactivity Section. The cross section obtained is $4.8 \pm 0.1 \times 10^{-29} \text{ cm}^2$. The error has almost equal contributions from counting statistics, uncertainties in the detector efficiency, and the monitor calibration as well as that arising from the positioning of the target relative to the Ge(Li) detector.

This result is to be compared with the cross section of $5.1 \pm 0.2 \times 10^{-29} \text{ cm}^2$ for 30 MeV electrons obtained by counting protons. Since the ^{62}Ni target has a 0.46% contamination of ^{58}Ni , having a much larger proton yield, the corrected $^{62}\text{Ni}(e, p)$ cross section would be $5.0 \pm 0.2 \times 10^{-29} \text{ cm}^2$, in good agreement with the value $4.8 \pm 0.1 \times 10^{-29} \text{ cm}^2$ obtained in the activation experiment. This exercise lends confidence to the absolute values reported in this paper.

C. The (e, α) cross sections

As has already been pointed out, α particles were detected simultaneously with the protons. The analysis of the results, however, turned out to be more involved. The yield curves for 8 MeV alphas emitted by ^{58}Ni at the angles 48°, 90°, and 132° are shown in Fig. 9. The full curves are drawn to guide the eye. The angular distribution for these particles peaks at 90° and within the accuracy of these measurements is symmetric about 90°. As with the proton data, these have been integrated over the α -particle energy spectra and over angle to obtain $\sigma_{e, \alpha}(E_0)$ which is displayed in Figs. 10 and 11. The angular distribution may be written as

$$\sigma(\theta, E_0) = \sigma(90^\circ) [A(E_0) + B(E_0) \sin^2 \theta], \quad (3)$$

where the functions $A(E_0)$ and $B(E_0)$ were determined empirically:

$$\begin{aligned} A(E_0) &= 0.49 + 8.3 \times 10^{-3} E_0, \\ B(E_0) &= 0.51 - 8.3 \times 10^{-3} E_0. \end{aligned} \quad (4)$$

It was not possible to fit the $\sigma_{e, \alpha}(E_0)$ and $Y_{e, \alpha}(E_0)$ data using the electric dipole virtual photon spectrum. This is illustrated in Fig. 10. As has already been indicated¹² by the $^{54}\text{Fe}(\alpha, \gamma_0)^{58}\text{Ni}$ experiment, the (γ, α) cross section has an important electric quadrupole component. For the three nickel isotopes, Figs. 11–13 show the measured cross sections $\sigma_{e, \alpha}(E_0)$, the yields $Y_{e, \alpha}(E_0)$, and the fits from which the $E1$ and $E2$ (γ, α) cross sec-

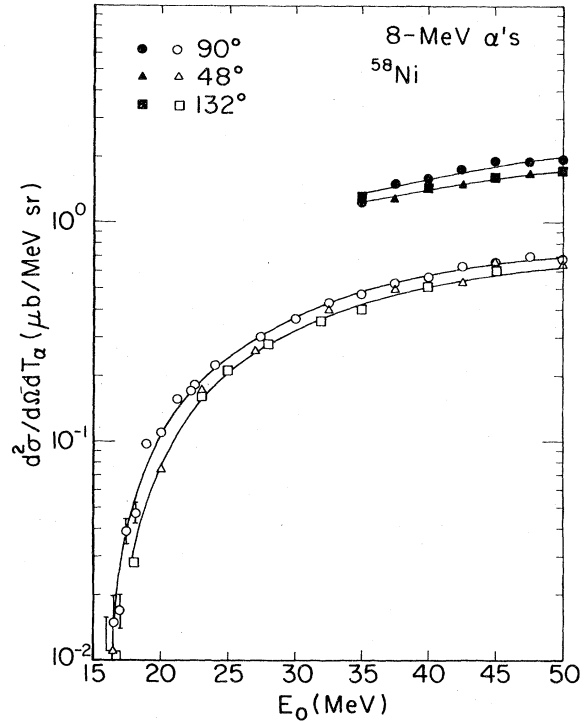


FIG. 9. The differential cross section $d^2\sigma/dT_\alpha d\Omega$ for the production of 8 MeV α particles from ^{58}Ni as a function of total incident electron energy E_0 . The data were taken at three angles: 90° (circles), 48° (triangles), and 132° (squares). The upper points refer to the yields resulting from electro plus photodisintegration when a 0.217 g/cm² tantalum radiator was interposed in the incident electron beam. The curves drawn through the points are merely to guide the eye.

tions were derived when the Davies-Bethe-Maximon bremsstrahlung cross section was used. The $E2$ strength occurs in a single bin extending from 14 to 20 MeV. It is located at the energy of the isoscalar $E2$ resonance and its strength is great enough to imply that α emission is an important decay mode for this resonance.

Table IV compares the percentages of the $E1$ and $E2$ sums in the α channel when the Schiff and Davies-Bethe-Maximon bremsstrahlung cross sections are used in the data analysis. It shows that the $E1$ strength in the α channel is not very important whereas the $E2$ strength is quite appreciable. In comparing these intensities one needs to recall that one isoscalar $E2$ sum in ^{60}Ni at 17 MeV represents 13 MeV mb, or only 1.5% of a dipole sum. We are only able to detect this $E2$ strength because of the steep rise of the virtual photon spectrum at low virtual photon energies. The $E2$ strengths obtained in this analysis are significantly smaller than those reported earlier,^{1,2} primarily because in the former analysis no cor-

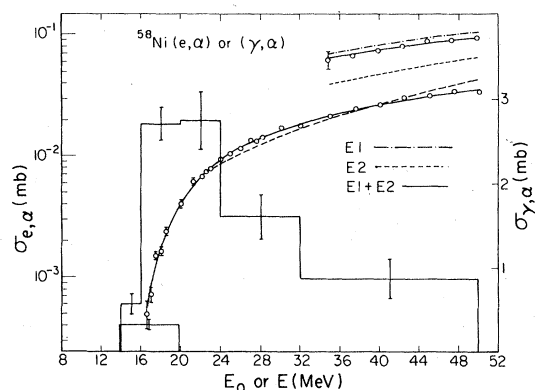


FIG. 10. The measured $\sigma(e, \alpha)$ (left-hand scale) for ^{58}Ni as a function of total incident electron energy E_0 . The upper circles represent the electro plus photodisintegration yield obtained when the 0.217 g/cm^2 tantalum foil was interposed in the incident electron beam. The full curves are the best fits that could be obtained for $\sigma_{e, \alpha}(E_0)$ and the yield $Y_{e, \alpha}(E_0)$ by folding the histograms representing the $E1$ and $E2$ components of the (γ, α) cross sections (right-hand scale) with the $E1$ and $E2$ virtual photon spectra in Eqs. (1) and (2). The Davies-Bethe-Maximon bremsstrahlung cross section has been used in this fit. The $E2$ strength is located in a single bin extending from 14 to 20 MeV. The dashed and dashed-dotted curves show the result of assuming $E2$ or $E1$ excitations alone.

rection was made for the change in geometry when the radiator was in.

The α particles emitted following $E1$ absorption must populate mainly levels 3.5 to 6.5 MeV above the ground state. There are, of course, individual differences for the three isotopes, since they have

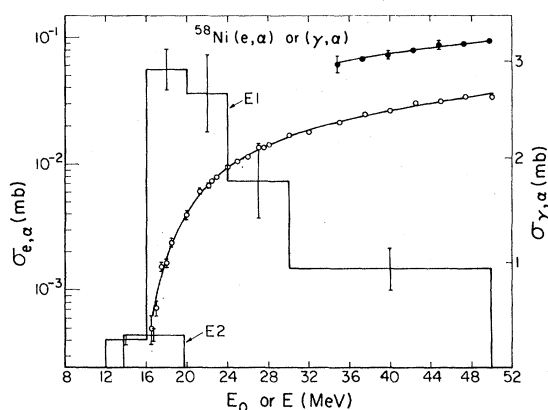


FIG. 11. The $^{58}\text{Ni}(e, \alpha)$ (open circles) cross section (left-hand scale) corrected yield (closed circles) obtained with radiator in. The curves through the points result from combining the histograms, representing the $E1$ and $E2$ (γ, α) cross sections (right-hand scale), in Eqs. (1) and (2) with the $E1$ and $E2$ virtual photon spectra and making use of the Davies-Bethe-Maximon cross section.

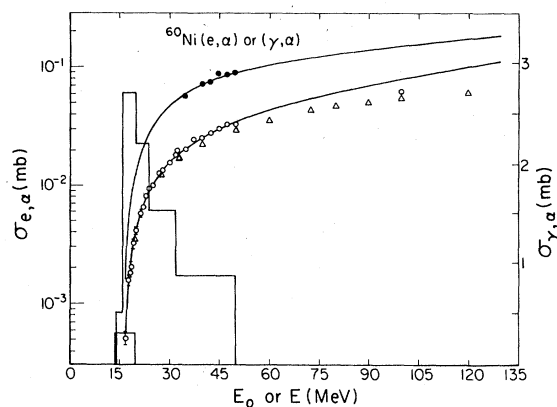


FIG. 12. The measured $\sigma_{e, \alpha}(E_0)$ for ^{60}Ni as a function of total incident electron energy E_0 (open circles). The full circles represent the electro plus photodisintegration yield obtained when the 0.217 g/cm^2 foil was interposed in the incident electron beam and the triangles show the data of Ref. 25. The smooth curves through the points result from combining the histograms, representing the $E1$ and $E2$ (γ, α) cross sections (right-hand scale), in Eqs. (1) and (2) with the $E1$ and $E2$ virtual photon spectra and making use of the Davies-Bethe-Maximon bremsstrahlung cross section. These integrals have been extended to 130 MeV assuming that the (γ, α) cross section is zero above 50 MeV. That the measured cross sections lie below this curve probably stems from the failure of the long wavelength approximation.

different separation energies, but, in any event, the level density in the residual nucleus is great enough so that several or many levels may be populated. The situation is quite different for the

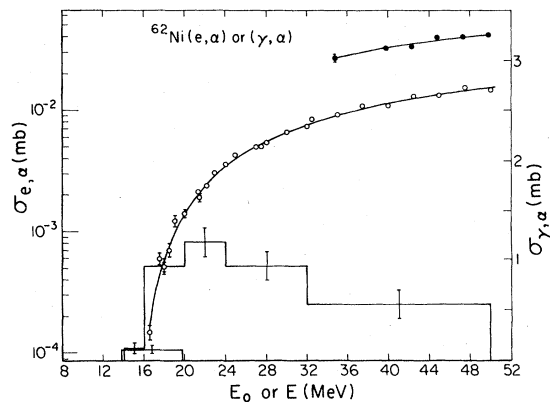


FIG. 13. The measured $\sigma(e, \alpha)$ for ^{62}Ni (open circles) as a function of total incident electron energy E_0 (left-hand scale). The full circles are electro plus photodisintegration yields obtained when the 0.217 g/cm^2 tantalum foil was interposed in the incident electron beam. The smooth curves through the points result from combining the histograms, representing the $E1$ and $E2$ (γ, α) cross sections (right-hand scale), in Eqs. (1) and (2) with the $E1$ and $E2$ virtual photon spectra and making use of the Davies-Bethe-Maximon cross section.

shape of the $E0$ and $E2$ virtual photon spectra it is not surprising that they do not result in similar electrodisintegration cross sections. If we assume that the (e, α) cross section in ^{58}Ni results from $E1$ and $E0$ absorption, place the $E0$ strength at $80A^{-1/3}$ MeV in a bin extending from 18 to 23 MeV, then we arrive at a poor fit to the electrodisintegration data and an $E0$ strength consistent with zero. Electrons of energies up to 50 MeV simply cannot transfer enough momentum to produce $E0$ excitations intense enough to be observed in this experiment.

E. Failure of the long wavelength approximation

In a recent paper Flowers *et al.*²⁵ have reported on a very similar experiment in which the $^{60}\text{Ni}(e, \alpha)$ reaction was studied for electron energies of up to 120 MeV. Their cross sections are shown as triangles in Fig. 12 to illustrate the good agreement between the two experiments in the region in which they overlap. The fits to the data of Figs. 11–13 have been made using the data points up to 50 MeV. When the integrals are evaluated up to electron energies of 120 MeV, the calculated cross section lies well above the experimental data points. There is no way to change the multipole composition of the absorption cross section to fit the higher energy points without destroying the fit to the $\sigma_{e,\alpha}(E_0)$ below 50 MeV and the electro plus photodisintegration yield. This discrepancy, which was also found for ^{58}Ni and ^{62}Ni , may very well result from using the long wavelength approximation.

To study the failure of the long wavelength approximation we have measured the (e, p) and (e, α) cross sections for the nickel isotopes at 100 MeV, $\sigma(\text{meas})$ of Tables V and VI. These are compared with the result obtained by evaluating the integral of Eq. (1) to 100 MeV using the photonuclear cross section already determined up to 50 MeV $\sigma(\text{calc})$. This is a lower limit since the photonuclear cross sections were taken to be zero between 50 and 100 MeV. [The results labeled $\sigma(\text{corr})$ will be described later.] In all cases the measured (e, p) cross section coincided with the result of the integration, in which the electric dipole virtual photon spectrum was used, if a very small amount of

TABLE V. $\sigma_{e,p}$ at 100 MeV.

Nucleus	$\sigma_{e,p}(\text{meas})$ (mb)	$\sigma_{e,p}(\text{calc})$ (mb)	$\sigma_{e,p}(\text{corr})$ (mb)
^{58}Ni	1.15 ± 0.02	1.10	0.98
^{60}Ni	0.50 ± 0.01	0.47	0.42
^{62}Ni	0.24 ± 0.01	0.22	0.19

TABLE VI. $\sigma_{e,\alpha}$ at 100 MeV.

Nucleus	$\sigma_{e,\alpha}(\text{meas})$ (mb)	$\sigma_{e,\alpha}(\text{calc})$ (mb)	$\sigma_{e,\alpha}(\text{corr})$ (mb)
^{58}Ni	0.069 ± 0.002	0.084	0.063
^{60}Ni	0.063 ± 0.002	0.081	0.060
^{62}Ni	0.033 ± 0.001	0.036	0.027

absorption between 50 and 100 MeV is allowed. The measured (e, α) cross sections, on the other hand, are much too small to agree with the result of folding the $E1$ and $E2$ cross sections with the virtual photon spectra that coincide with the measurements below 50 MeV. We believe that this is a direct consequence of the failure of the long wavelength approximation.

These results show that the electric dipole virtual photon analysis for nickel succeeds at least up to electron energies of 100 MeV and that when electric quadrupole absorption is important, the analysis fails above 50 MeV. As has already been pointed out by both Barber⁵ and Isabelle and Bishop,⁶ the long wavelength approximation will fail when large momentum transfers become important and the $E2$ matrix elements have sizable longitudinal components. This is illustrated in Fig. 16 where we plot the ratios of the numbers of

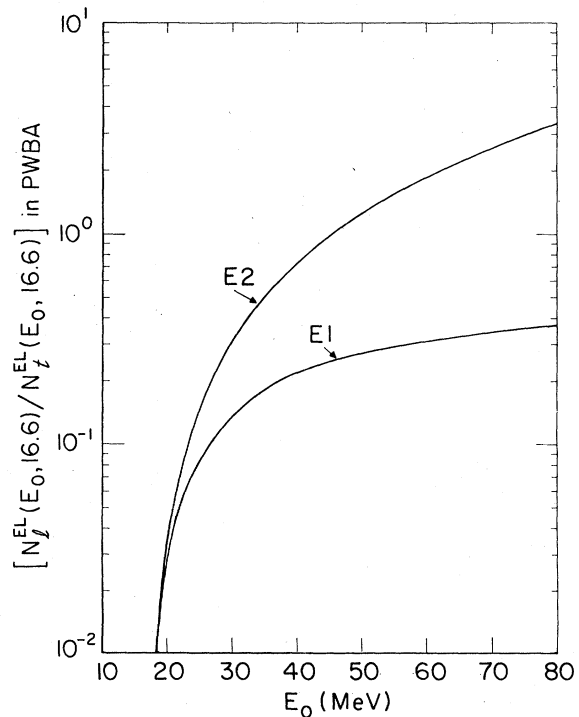


FIG. 16. The ratio of the intensities of 16.6 MeV longitudinal to transverse photons in the $E1$ and $E2$ plane-wave virtual photon spectra as a function of E_0 .

16.6 MeV longitudinal to transverse photons in the $E1$ and $E2$ plane-wave virtual photon spectra^{41,42} as a function of electron energy. The longitudinal parts never make an important contribution to the $E1$ virtual photon spectra, but the longitudinal components of the $E2$ become as large as the transverse for electrons of energy near 50 MeV.

In the limit of small momentum transfer $q \rightarrow E$, the reduced matrix element associated with a photonuclear process is identical to the reduced matrix element for the corresponding electro-nuclear process. This identity allows us to write Eq. (1) which defines the virtual photon spectrum. The transition probabilities $B(\lambda L, q)$ occurring in the electron scattering cross section vary with q as the squares of the spherical Bessel functions $j_L(qR)$. The long wavelength approximation⁴³ consists in replacing $j_L(qR)$ by the first term in its expansion, i.e.,

$$j_L(qR) \cong (qR)^L / (2L+1)!! \quad (5)$$

We have made a correction to the virtual photon spectra in an attempt to take this failure into account. This correction consists in multiplying $N^{EL}(E_0, E, Z)$ inside the integrals of Eq. (1) and (2) by the quantity

$$F^{EL}(qR) = \left[\left(\frac{E}{q} \right)^L \frac{j_L(qR)}{j_L(ER)} \right]^2. \quad (6)$$

The average values of q^2 participating in the interaction were estimated by comparing the plane-wave virtual photon spectrum for the L involved, with that for the next higher multiple. Since the electron scattering cross section is proportional to q^{2L} , the longitudinal term having an additional factor of $L/(L+1)$,

$$N_i^{E(L+1)}/N_i^{EL} = \langle q^2 \rangle_i / E^2 \quad (7)$$

and

$$N_i^{E(L+1)}/N_i^{EL} = [(L+1)^2/L(L+2)] \langle q^2 \rangle_i / E^2. \quad (8)$$

Then

$$\frac{\langle q^2 \rangle}{E^2} = \frac{N_i^{E(L+1)} + [L(L+2)/(L+1)^2] N_i^{EL}}{N_i^{EL} + N_i^{EL}}. \quad (9)$$

For the transition radius R , we have used $1.2A^{1/3}$ $(3/5)^{1/2} = 0.93A^{1/3}$ fm. This procedure underestimates the correction to the virtual photon spectrum since the average values of the momentum transfer associated with the real interaction, in which the Coulomb distortion is taken into account, are much larger than those included in the plane-wave result. It can, nevertheless, be used as a guide and yields results consistent with those of Shotter⁴⁴ whose estimates are based on the generalized Helm model.^{45,46} Our technique has the advantage over the explicit calculations of Shotter

in that it can also be used to estimate the finite size correction to the distorted-wave virtual photon spectra. The distorted-wave virtual photon spectra cannot be decomposed into longitudinal and transverse components; only the total virtual photon spectra are calculated. However, to the extent that $L(L+2)/(L+1)^2 \approx 1$, $\langle q^2 \rangle/E^2$ is still given by $N^{E(L+1)}/N^{EL}$. For Ni, the differences between finite size corrections using plane- and distorted-wave virtual photon spectra to estimate $\langle q^2 \rangle/E^2$ are not significant; however, for heavier targets the differences are very important.

When these modified DWBA virtual photon spectra were used in the analysis of our data, the $E1$ components were left essentially unchanged but the $E2$ intensities in the derived (γ, α) cross sections were increased. The results obtained from the (e, α) cross sections are given in Table VII using the histogram fit and the two choices for the bremsstrahlung cross section as before. When the integral is evaluated to 100 MeV using the cross sections derived up to 50 MeV, we obtain the cross sections given in column 4 of Tables V and VI. It may be seen that the corrected (e, p) cross section will now permit slightly greater (γ, p) cross sections in the range 50–100 MeV and the corrected (e, α) cross section is now reasonable, i.e., less than the measured one, allowing a small (e, α) cross section for E_0 in excess of 50 MeV.

IV. CONCLUSIONS

We have shown that the (e, p) cross sections for ^{58}Ni , ^{60}Ni , and ^{62}Ni can be described in terms of electric dipole (γ, p) cross sections through the DWBA virtual photon spectra. Our experiment is sensitive to the energy and strength but not to the detailed shape of the (γ, p) cross sections. The (e, α) cross sections have been shown to result from both $E1$ and $E2$ absorption. The $E2$ giant resonance in the nickel isotopes is located at an energy such that the α particles emitted can survive the Coulomb barrier; in very heavy nuclei this would not occur. Up to 50 MeV the DWBA $E2$ virtual photon spectra for Ni are adequate though size effects seem to be important at 100 MeV;

TABLE VII. Percentage of the $E1$ and $E2$ sums in the α channel if nuclear size corrections are made.

Nucleus	$E1$		$E2$	
	Schiff	D-B-M	Schiff	D-B-M
^{58}Ni	4.9 ± 0.5	6.1 ± 0.6	31 ± 3	21 ± 3
^{60}Ni	4.5 ± 0.7	5.5 ± 0.7	31 ± 5	21 ± 5
^{62}Ni	2.4 ± 0.3	2.9 ± 0.3	13 ± 2	8 ± 2

these effects can be expected to be important for lower electron energies in heavier targets.

The α decays of the isoscalar $E2$ giant resonance for ^{58}Ni and ^{62}Ni have been measured in the $(\alpha, \alpha'\alpha'')$ experiments. Our results are in agreement with the upper limit quoted by Knöpfle⁴⁷ but are larger than the result of Collins *et al.*⁴⁸ Almost all of the protons measured in the present experiment come from the electric dipole giant resonance. In fact, if we add our derived integrated (γ, p) cross sections of Table III for ^{58}Ni and ^{60}Ni to the neutron yield cross sections tabulated by Berman and Fultz⁴⁹ we obtain, respectively, 1.15 and 1.14 dipole sums. On the other hand, since the electric dipole (e, p) cross section is so important, it is very difficult to exclude that a small part of the proton yield results from $E2$ absorption. It could be as much as an $E2$ sum.

Though the ultimate experiment would be one in which the scattered electron is measured in coincidence with the outgoing nucleon or α particle, the experiment described above represents a new and powerful method for determining the multipolarities of the giant resonances without the backgrounds that plague the hadron scattering experiments or the radiation tails of inelastic electron scattering. Since the electromagnetic interaction is known, a comparison of electrodisintegration data with that obtained using heavier projectiles may lead to a better model for the inter-

pretation of the inelastic hadron scattering experiments.

The biggest problem with the virtual photon theory basic to this analysis is the lack of knowledge concerning nuclear size effects. These enter when the long wavelength approximation is no longer valid and are much more important for $E2$ excitations than for $E1$. It transpires that for the energies of interest here the size effects are almost negligible for the $E1$ spectra but the $E2$ spectra must be used with caution for electron energies above 50 MeV.

ACKNOWLEDGMENTS

The authors wish to thank S. Penner and E. G. Fuller for many interesting discussions, J. W. Lightbody, Jr. and X. K. Maruyama for their analysis of the ^{60}Ni targets, and F. Schima and X. K. Maruyama for their help with the activation experiment. R. O. Owens and L. C. Maximon contributed some very useful suggestions. They also thank the Pontificia Universidade Catolica do Rio De Janeiro for the computer time that produced the virtual photon spectra. The work of E. W. was supported in part by Fundacao de Amparo a Pesquisa do Estado de Sao Paulo. The work of R. G. L. was supported by Deutsche Forschungsgemeinschaft.

*On leave from the University of Sao Paulo.

†On leave from Max-Planck-Institute für Chemie, Mainz, Germany.

¹E. Wolyneć, W. R. Dodge, and E. Hayward, Phys. Rev. Lett. **42**, 27 (1979).

²E. Hayward, Lecture Notes in Physics **108**, 300 (1979).

³W. W. Gargaro and D. S. Onley, Phys. Rev. C **4**, 1032 (1971).

⁴C. W. Soto Vargas, D. S. Onley, and L. E. Wright, Nucl. Phys. **A288**, 45 (1977).

⁵W. C. Barber, Annu. Rev. Nucl. Sci. **12**, 1 (1962).

⁶D. B. Isabelle and G. R. Bishop, Nucl. Phys. **45**, 209 (1963).

⁷L. I. Schiff, Phys. Rev. **96**, 765 (1954).

⁸B. F. Gibson and H. T. Williams, Nucl. Phys. **A163**, 193 (1971).

⁹I. C. Nascimento, E. Wolyneć, and D. S. Onley, Nucl. Phys. **A246**, 210 (1975).

¹⁰M. N. Martins, E. Wolyneć, and G. Moscati, Phys. Rev. C **16**, 613 (1977).

¹¹S. S. Hanna, in *Photonuclear Reactions*, edited by S. Costa and C. Schaerf (Springer, New York, 1977), p. 275.

¹²L. Meyer-Schützmeister, R. E. Segel, K. Raghuma-

than, P. T. Debevec, W. R. Wharton, L. L. Rutledge, and T. R. Ophel, Phys. Rev. C **17**, 56 (1978).

¹³W. R. Dodge and W. C. Barber, Phys. Rev. **127**, 1746 (1962).

¹⁴W. C. Barber and V. J. Vanhuyse, Nucl. Phys. **16**, 381 (1960).

¹⁵J. J. Murphy II, H. S. Gehrhardt, and D. M. Skopik, Nucl. Phys. **A277**, 69 (1977).

¹⁶J. J. Murphy II, D. M. Skopik, J. Asai, and J. Uegaki, Phys. Rev. C **18**, 736 (1978).

¹⁷W. R. Dodge and H. Vander Molen, *Proceedings of the Second International Conference on Clustering Phenomena in Nuclei, College Park, Maryland, 1975*, edited by D. A. Goldberg, J. B. Marion, and S. J. Wallace (National Technical Information Service, Springfield, Virginia, 1975).

¹⁸T. Tamae, T. Urano, and M. Sugawara, in *Sendai Conference on Electro- and Photoexcitations*, edited by Y. Kawazoe (Research Report of Laboratory of Nuclear Science, Tohoku University, Tomizawa, Sendai, Japan, 1977), p. 231.

¹⁹A. G. Flowers, D. Poranford, J. C. McGeorge, A. C. Shotton, P. Thorley, C. H. Zimmerman, R. O. Owens, and J. S. Pringle, Phys. Rev. Lett. **43**, 323 (1979).

- ²⁰B. S. Ishkhanov, I. M. Kapitonov, Im. M. Piskarev, V. G. Shevchenko, and O. P. Shevchenko, *Yad. Fiz.* **11**, 485 (1970) [*Sov. J. Nucl. Phys.* **11**, 272 (1970)].
- ²¹B. S. Ishkhanov, I. M. Kapitonov, V. G. Shevchenko, V. I. Shvedunov, and V. V. Varlemov, *Nucl. Phys.* **A283**, 307 (1977).
- ²²J. H. Carver and W. Turchinets, *Proc. R. Soc. London* **73**, 585 (1959).
- ²³H. Miyase, S. Oikawa, A. Suzuki, J. Uegaki, T. Saito, M. Sugawara, and K. Shoda, *Proceedings of the International Conference on Photonuclear Reactions and Applications*, edited by B. L. Berman (Lawrence Livermore Laboratory, Livermore, California, 1973), Vol. I, p. 553.
- ²⁴E. M. Diener, J. F. Amann, P. Paul, and S. L. Blatt, *Phys. Rev. C* **3**, 2303 (1971).
- ²⁵A. G. Flowers, A. C. Shotter, D. Branford, J. C. McGeorge, and R. O. Owens, *Phys. Rev. Lett.* **40**, 709 (1978).
- ²⁶G. S. Foote, D. Branford, R. A. I. Bell, and R. B. Watson, *Nucl. Phys.* **A220**, 505 (1974).
- ²⁷D. M. Skopik and W. R. Dodge, *Phys. Rev. C* **6**, 43 (1972).
- ²⁸K. Min and T. A. White, *Phys. Rev. Lett.* **21**, 1200 (1968).
- ²⁹D. G. Owen, E. G. Muirhead, and B. M. Spicer, *Nucl. Phys.* **A140**, 523 (1970).
- ³⁰S. C. Fultz, R. A. Alvarez, B. L. Berman, and P. Meyer, *Phys. Rev. C* **10**, 608 (1974).
- ³¹A. G. Flowers, private communication.
- ³²L. I. Schiff, *Phys. Rev.* **83**, 252 (1951).
- ³³H. Davies, H. A. Bethe, and L. C. Maximon, *Phys. Rev.* **93**, 788 (1954).
- ³⁴J. L. Matthews and R. O. Owens, *Nucl. Instrum. Methods* **111**, 157 (1973).
- ³⁵H. W. Koch and J. W. Motz, *Rev. Mod. Phys.* **31**, 920 (1959).
- ³⁶H. K. Tseng and R. H. Pratt, *Phys. Rev. A* **19**, 1525 (1979).
- ³⁷R. L. Auble, *Nucl. Data Sheets* **16**, 1 (1975).
- ³⁸F. J. Kline and Evans Hayward, *Phys. Rev. C* **17**, 1531 (1978).
- ³⁹A. T. Hirshfeld, D. D. Hoppes, and F. J. Schima, *Proceedings of the ERDA X- and Gamma-Ray Symposium*, Ann Arbor, Mich., 1976 (unpublished), p. 60.
- ⁴⁰E. Hayward, *Lecture Notes in Physics* **61**, 372 (1977).
- ⁴¹J. A. Thie, C. J. Mullin, and E. Guth, *Phys. Rev.* **87**, 962 (1952).
- ⁴²R. H. Dalitz and D. R. Yennie, *Phys. Rev.* **105**, 1598 (1957).
- ⁴³K. Alder, A. Bohr, T. Huus, B. Mottelson, and A. Winter, *Rev. Mod. Phys.* **28**, 432 (1956).
- ⁴⁴A. C. Shotter, *J. Phys. G* **5**, 371 (1979).
- ⁴⁵R. H. Helm, *Phys. Rev.* **104**, 1466 (1956).
- ⁴⁶M. Rosen, R. Raphael, and H. Überall, *Phys. Rev.* **163**, 927 (1967).
- ⁴⁷K. T. Knöpfle, *Lecture Notes in Physics* **108**, 311 (1979).
- ⁴⁸M. T. Collins, C. C. Chang, S. L. Tabor, J. R. Wu, and M. D. Glascock, *Bull. Am. Phys. Soc.* **23**, 506 (1978).
- ⁴⁹B. L. Berman and S. C. Fultz, *Rev. Mod. Phys.* **47**, 713 (1975).